NASA/TP–2010-216212

A Rat Body Phantom for Radiation Analysis

Garry D. Qualls and Martha S. Clowdsley
Langley Research Center, Hampton, Virginia

Tony C. Slaba and Steven A. Walker
Old Dominion University, Norfolk, Virginia

March 2010

NASA STI Program . . . in Profile

Since its founding, NASA has been dedicated to the advancement of aeronautics and space science. The NASA scientific and technical information (STI) program plays a key part in helping NASA maintain this important role.

The NASA STI program operates under the auspices of the Agency Chief Information Officer. It collects, organizes, provides for archiving, and disseminates NASA's STI. The NASA STI program provides access to the NASA Aeronautics and Space Database and its public interface, the NASA Technical Report Server, thus providing one of the largest collections of aeronautical and space science STI in the world. Results are published in both non-NASA channels and by NASA in the NASA STI Report Series, which includes the following report types:

- TECHNICAL PUBLICATION. Reports of completed research or a major significant phase of research that present the results of NASA programs and include extensive data or theoretical analysis. Includes compilations of significant scientific and technical data and information deemed to be of continuing reference value. NASA counterpart of peer-reviewed formal professional papers, but having less stringent limitations on manuscript length and extent of graphic presentations.

- TECHNICAL MEMORANDUM. Scientific and technical findings that are preliminary or of specialized interest, e.g., quick release reports, working papers, and bibliographies that contain minimal annotation. Does not contain extensive analysis.

- CONTRACTOR REPORT. Scientific and technical findings by NASA-sponsored contractors and grantees.

- CONFERENCE PUBLICATION. Collected papers from scientific and technical conferences, symposia, seminars, or other meetings sponsored or co-sponsored by NASA.

- SPECIAL PUBLICATION. Scientific, technical, or historical information from NASA programs, projects, and missions, often concerned with subjects having substantial public interest.

- TECHNICAL TRANSLATION. English-language translations of foreign scientific and technical material pertinent to NASA's mission.

Specialized services also include creating custom thesauri, building customized databases, and organizing and publishing research results.

For more information about the NASA STI program, see the following:

- Access the NASA STI program home page at *http://www.sti.nasa.gov*

- E-mail your question via the Internet to help@sti.nasa.gov

- Fax your question to the NASA STI Help Desk at 443-757-5803

- Phone the NASA STI Help Desk at 443-757-5802

- Write to:
  NASA STI Help Desk
  NASA Center for AeroSpace Information
  7115 Standard Drive
  Hanover, MD 21076-1320

NASA/TP–2010-216212

A Rat Body Phantom for Radiation Analysis

Garry D. Qualls and Martha S. Clowdsley
Langley Research Center, Hampton, Virginia

Tony C. Slaba and Steven A. Walker
Old Dominion University, Norfolk, Virginia

March 2010

Abbreviations

BFO	Blood Forming Organs
CAF	Computerized Anatomical Female
CAM	Computerized Anatomical Man
CT	Computed Tomography
FAX	Female Adult voXel model
GCR	Galactic Cosmic Rays
HZETRN	High charge (Z) and Energy TRaNsport
LEO	Low Earth Orbit
MAX	Male Adult voXel model
SPE	Solar Particle Event

Contents

Figures

Tables

Abstract

To reduce the uncertainties associated with estimating the biological effects of ionizing radiation in tissue, researchers rely on laboratory experiments in which mono-energetic, single specie beams are applied to cell cultures, insects, and small animals. To estimate the radiation effects on astronauts in deep space or low Earth orbit, who are exposed to mixed field broad spectrum radiation, these experimental results are extrapolated and combined with other data to produce radiation quality factors, radiation weighting factors, and other risk related quantities for humans. One way to reduce the uncertainty associated with such extrapolations is to utilize analysis tools that are applicable to both laboratory and space environments. The use of physical and computational body phantoms to predict radiation exposure and its effects is well established and a wide range of human and non-human phantoms are in use today. In this paper, a computational rat phantom is presented, as well as a description of the process through which that phantom has been coupled to existing radiation analysis tools. Sample results are presented for two space radiation environments.

1. Introduction

There are currently large uncertainties associated with estimates of the biological effectiveness of ionizing radiation in tissue [Cucinotta et al. 2006]. To help reduce these uncertainties, researchers rely upon laboratory experiments in which mono-energetic, single specie beams are applied to cell cultures, insects, and small animals – primarily rodents. Astronauts can be exposed to space radiation in the form of galactic cosmic rays (GCR), solar particle events (SPE), or trapped ions in low Earth orbit (LEO). Predicting their risk of carcinogenesis or other radiation-related health problems (heart disease, cataracts, acute radiation syndrome, etc.) that result from their exposure is determined mainly by the results of laboratory beam experiments. Consequently, there are many situations in which the laboratory experiments must be extrapolated for space applications. An obvious example is the use of insects and small animals instead of human subjects in beam exposure studies. The connection between the biological effects induced in insects and small animals, and the biological effects induced in humans by the same radiation is not always clear. One way of reducing this uncertainty is to utilize risk analysis software that can be used interchangeably in laboratory or space environments. Various human phantoms have been employed for this task [Zaidi and Xu 2007], and some rodent phantoms have also been developed [Zaidi and Xu 2007]. In this paper, a new rat phantom is presented that has been coupled with the radiation analysis tools used by NASA.

Slaba et al. [2009] have discussed in detail the coupling of the human phantoms CAM (Computerized Anatomical Man) [Billings et al. 1973], CAF (Computerized Anatomical Female) [Yucker et al. 1990, 1992], MAX (Male Adult voXel model) [Kramer et al. 2003], and FAX (Female Adult voXel model) [Kramer et al. 2004] to the deterministic transport code HZETRN (High charge (Z) and Energy TRaNsport) [Wilson et al. 1991; Slaba et al. 2008]. A brief summary is given here. In order to calculate the dose at a single target point, ray tracing techniques are used to determine the directional distribution of tissues and shielding materials surrounding the target point. HZETRN combines this distribution of tissue and shield material thicknesses with a radiation environment model to estimate the dose at the target point. Mass averaged organ doses are computed by repeating this process for many target points within a given organ and then averaging. For the purposes of this report, the term "dose" is used as a generic term to refer to exposure quantities such as flux, dose, dose equivalent, or gray-equivalent.

Using this approach, it is possible to couple a variety of computational human and animal phantoms to HZETRN and estimate exposure quantities within various tissues. To get accurate results for a particular phantom, a ray tracing algorithm that can accurately calculate the directional distribution of tissues surrounding a given target point is required. Additionally, for organ-averaged quantities, a point distribution method is needed that accurately and uniformly samples the individual tissue. This paper describes the development of the computational rat phantom, the ray tracing techniques, and the point distribution methods used to couple the phantom to HZETRN. Sample results for a whole rat and four

individual rat organs are presented to demonstrate the applicability of a rat phantom to space radiation analyses.

2. Description of Rat Data

The phantom tissue model is based upon a full-body CT (Computed Tomography) scan of an adult male rat. The rat was anesthetized at the time of the scan and was lying on its back, as shown in Figure 1. Rolls of cloth were placed on either side of its spine to support it and align its body axially for the scan. The rat and support cloths were lying on a flat wooden platform that is visible in the lower part of the scanned volume.
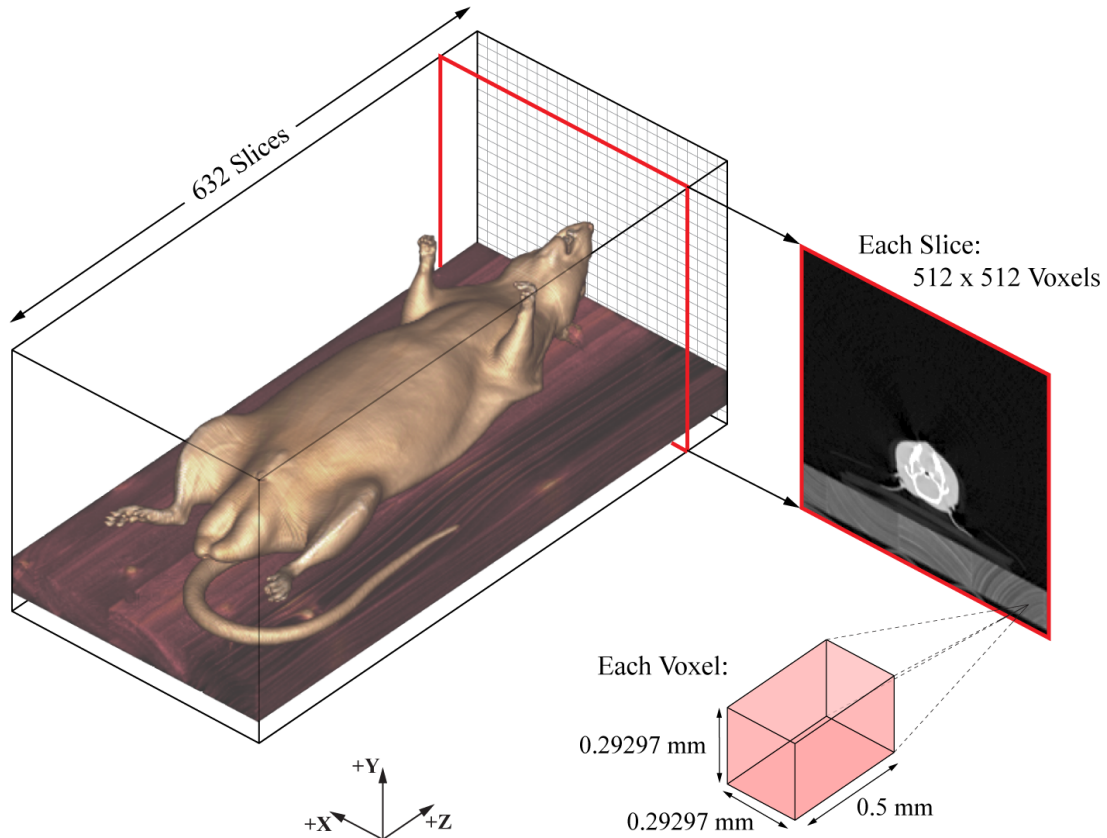

Figure 1. On the left is a volume rendering of the complete CT scan data set showing the anesthetized rat lying on its back, supported by a wooden platform, inside the rectangular volume that was scanned. A single CT scan image or "slice" that intersects the head is also shown, along with an illustration of the voxel dimensions for this data.

CT-scans are computed as a series of discrete images or "slices" that typically have fixed spacing along the length of the body being scanned. Each slice of CT-scan data is an evenly spaced, rectangular grid of points with a single data value specified for each grid point. This data value is known as a "Hounsfield number". Hounsfield numbers correlate directly to the amount of X-ray energy attenuation caused by the tissue associated with each grid point. CT-scan machines are calibrated using a reference sample of pure water. The machine is tuned so that air within the volume being scanned produces a Hounsfield number of -1000 and the reference water sample produces a Hounsfield number of zero. This calibration provides a standard baseline so that CT-scans are comparable across different scanners and X-ray beam energy spectra. For this particular data set, the underlying wooden table was removed at run-time

by the analysis software, without modifying the original rat data files. Also, the 98th CT-scan data slice was missing from the original data and was replaced by copying data from the 97th slice.

For this research, the spacing between adjacent slices is used to define the thickness of each slice, which is the convention used for most CT-scan visualizations. Each slice of the rat data used in this study can be thought of as a square image with dimensions of 512 pixels by 512 pixels. Since each slice has thickness however, each pixel expands from being a two-dimensional section of an image to being a three-dimensional section of a volume and is thus called a "voxel". Physically, each slice is 150 mm x150 mm, and 633 slices are stacked to represent a distance of 316.5 mm along the length of the rat. This results in a constant voxel size throughout the scanned volume that is 0.29297 mm x 0.29297 mm x 0.5 mm.

3. Description of Ray Tracing Process for CT-based Voxel Models

To accurately compute an organ-averaged dose for a selected tissue type in a voxel-based phantom, it is important to use a process that captures both the angular distribution of incoming radiation and the angular variation of the quantity and type of tissue surrounding the organ. A ray tracing approach is used to sample the directional distribution of the external radiation environment and the corresponding distribution of the body tissue surrounding discrete points within the phantom. For this approach, points are specified within the body phantom and a number of rays are "traced" away from each point. The distribution of rays is usually chosen for uniformity with which it samples the full 4π spherical solid angle. The total number of evenly distributed rays is usually chosen so that the angular spacing between adjacent rays is small enough to capture any meaningful variations in both the external environment and the distribution of body tissue that is providing shielding. During the ray tracing process, the amount and type of tissue is evaluated along each ray and stored for analysis. Many phantoms define voxel properties by specifying the tissue type and corresponding tissue density for each voxel. For a model that is based directly on CT data, however, relationships need to be established that relate the Hounsfield numbers to tissue types and densities.

Since the Hounsfield number represents the average absorption coefficient for each voxel of tissue, it correlates well with tissue density. A numerical curve fit was developed at NASA Langley in the early 1990's to capture this relationship. Reference values for specific body tissue densities were compared to the Hounsfield numbers from a full-body human CT-scan and a least-squares approach was used to fit the data. Extending the application of this human-based correlation to the rat yielded a total rat mass of 549.8 g. This mass is within the range of 300-800 g, which is considered normal for an adult male rat in a research environment [Poole 1986]. The nature of the data allows for geometric scaling by changing the voxel dimensions to produce a rat with any desired mass.

When interpreting CT-scans for medical diagnostic purposes, it is common for the scans to exhibit poor contrast between tissues that have similar densities. A CT image can be used to reliably differentiate between tissues that have the lower density of fat, soft tissues that have a density very close to that of water, and more dense bone structures that cover the full range of bone density in the human body. Thus, it is possible to use CT data to create a simple segmentation of voxel data into different density sets. Differentiating between non-tissue, soft tissue, and bone is relatively straightforward and the Hounsfield numbers chosen to represent the boundaries between these groups are shown in Figure 2.

Rat CT Slice 229
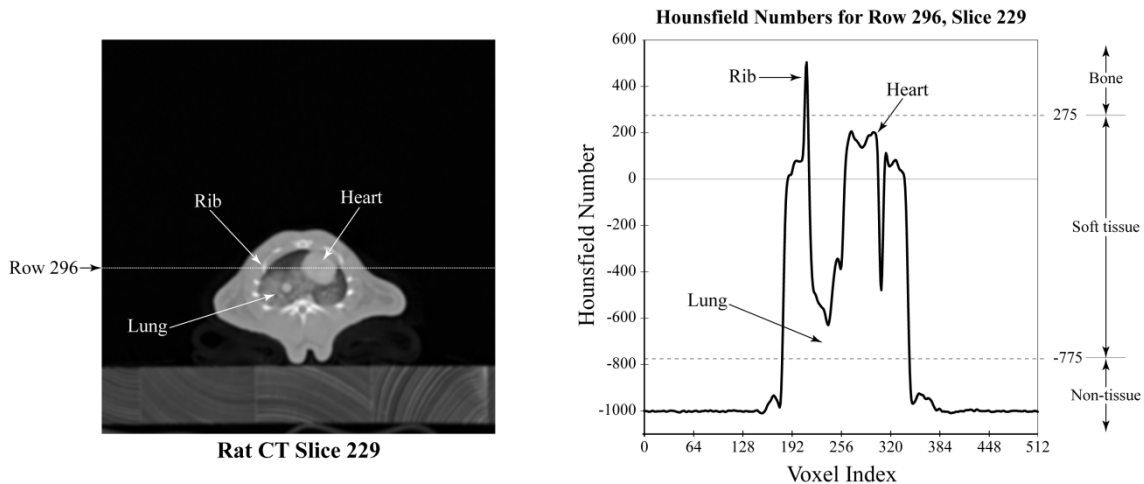
Hounsfield Numbers for Row 296, Slice 229

Figure 2. Rat CT Slice 229, including labels for some anatomic features, is shown on the left. Hounsfield numbers for row 296 of this slice are plotted on the right with corresponding anatomic feature labels. Specific Hounsfield number ranges used to classify voxels as non-tissue, soft tissue, or bone are illustrated along the right edge of the plot.

The ray tracing software used for analysis produced three different types of output. The simplest output type represented the total tissue column areal density along each ray as a single value. This number was obtained by multiplying the volumetric density of each voxel and the length of the ray segment that fell inside that voxel. A second kind of output preserved only information related to the quantities of each tissue type that were found along each ray. For this output type, subtotals were kept for each tissue type along a ray and areal densities of bone, tissue, etc. were recorded, however, the order of the different tissue types along the ray was lost. The third, and most verbose, output type recorded the areal density of each contiguous segment of each tissue type along a ray. Since it is common for a ray to traverse many boundaries between different tissue types as it exits the body, this output file type generates comparatively large files.

In addition to cataloging the amount of tissue along each ray as it emanates from a point in the body, the ray tracer collected information about the tissue behind the point in order to support analyses that include the effects of backscattered radiation. This information about the backing tissue along each ray was supplied for each of the three output types described above.

4. Target Point Distribution Methods

In addition to distributing the rays around a target point evenly, it is important to distribute the target points throughout the tissue in such a way that the calculated results will accurately represent the mass-averaged dose for all tissue of that type in the body. Two different point distribution methods were used to sample the tissue types presented. The simplest approach used to distribute points was based upon an evenly spaced, orthogonal, three dimensional grid. Only grid points that were within voxels identified as tissue were used for analysis. This approach was used to calculate doses for the rat as a whole and to look at dose gradients within the rat tissue. A number of grid spacings were tested to find a spacing that was adequate.

A second point distribution method was used for calculating the organ-averaged doses. This approach was based upon methods originally used to create unstructured meshes in implicit geometries [Persson and Strang 2004], and its application to these types of problems is described in detail elsewhere [Slaba et al. 2009]. In summary, an unstructured tetrahedral mesh is created within the boundaries of an organ and the mesh properties are adjusted to achieve even spacing between mesh points in the organ's interior. As in the simpler, whole-rat approach, a number of mesh sizes were tested to find an adequate spacing for these analyses.
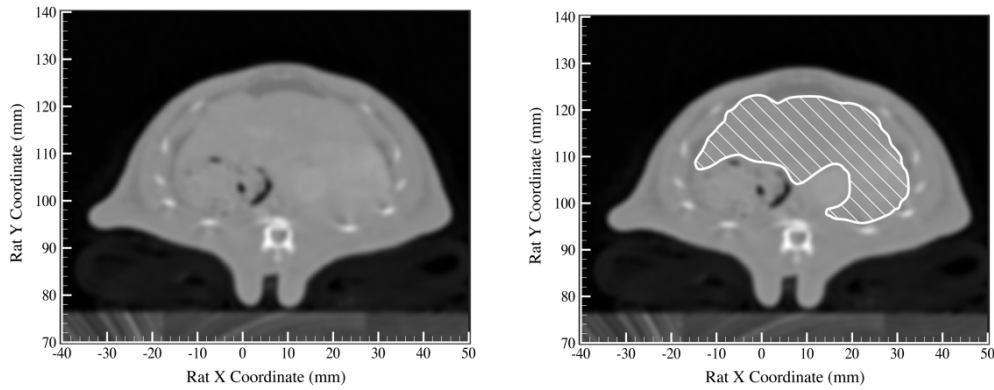
4

Figure 3. Detail of rat abdominal CT Slice 269 showing typical tissue contrast and the same slice with a region of interest defined for liver tissue.

Tissue segmentations were created for four different tissue types within the rat phantom: the brain, lungs, liver, and blood forming organs (BFO). Each segmented organ was created by examining the CT slices individually and manually creating maps that identified the voxels that belonged to each organ (see Figure 3). Figure 4 shows the location and extent of each of the four tissues within the rat.
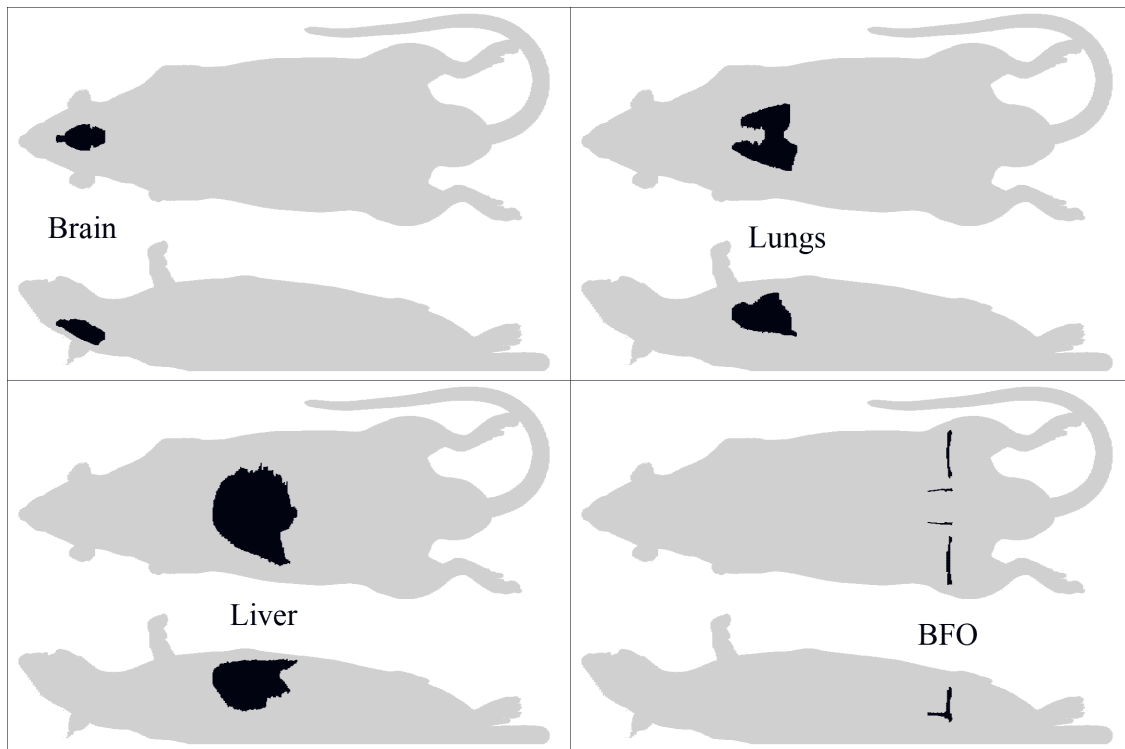

Figure 4. Top and side views of the brain, lungs, liver and BFO segmentations with segmented tissues shown as a black silhouettes against the grey full body rat outlines.

The brain and lungs were easily segmented since both are surrounded by tissues that are significantly more dense, providing good boundary contrast. In some areas, the rat liver is bounded by

other organs and muscle tissue with a similar density, making segmentation more difficult. With some experience, the high resolution and low noise of the original rat CT scan made it possible to discern boundaries by making multiple passes through the data to create topological consistency from slice to slice. The segmentation of BFO tissue was complicated by the very small size and low density of most of the rat bones. The rat pelvis, however, exhibited high bone density and comparatively large internal cavities for marrow. These volumes inside the pelvis were segmented, but due to their very small volume, the algorithms used to distribute points in the other organs were not applicable and dose points were distributed manually within them.

5. Sample Results

Sample results have been computed in the rat BFO, brain, liver, and lungs. External shielding geometries were defined as spherical aluminum shells with areal densities of 0.4 g/cm^2 or 20 g/cm^2. Two space radiation environments were applied isotropically to the spherical aluminum shells with the rat inside. The environments chosen were the 1977 solar minimum GCR spectrum [O'Neill 2006] and the August 1972 SPE as modeled by King [King 1974]. The dose values obtained in the four rat organs are given in Table 1 and the dose equivalent values are given in Table 2. The average BFO light particle fluence spectra (n, p, ^{2}H, ^{3}H, ^{3}He, ^{4}He) associated with the 20 g/cm^2 shield and SPE environment are shown in Figure 5.

Figures 6 and 7 are contour plots that illustrate the variation of dose equivalent within a single rat slice inside the 0.4 g/cm^2 shield for the SPE and GCR environments, respectively. Note that the ranges of dose equivalent values shown in the two plots are quite different. For the SPE environment shown in Figure 6, the dose equivalent values are large and cover a large range from approximately 1000 cSv at central points in the rat to approximately 7500 cSv on the surface of the rat. The August 1972 SPE was comprised of a large number of low and medium energy protons, the vast majority of which had energies less than 100 MeV. As these protons move through the rat tissue, they interact with the atoms making up the tissue and lose energy very quickly, primarily through ionization. This results in large changes in dose equivalent over small changes in tissue depth. Conversely, the GCR environment is made up of protons, alpha particles, and heavier charged ions with energies ranging from a few A MeV to approximately 50,000 A MeV with peak fluences around 1000 A MeV. The heavier and more energetic particles from this environment travel deeper into the tissue, resulting in a much smaller variation in dose equivalent values in the rat. Figure 7 shows that the daily dose equivalent rate in this rat slice varies from approximately 0.21 cSv at interior points to 0.26 cSv on the surface.

Table 1. Dose in rat tissues protected by spherical shielding, exposed to SPE and GCR environments. The unit for GCR dose is cGy/day, and the unit for SPE dose is cGy/event.

| | 1977 solar min GCR | | August 1972 King SPE | |
	0.4 g/cm^2	20 g/cm^2	0.4 g/cm^2	20 g/cm^2
BFO	0.060	0.057	780.7	9.6
Brain	0.060	0.056	1063.8	10.8
Liver	0.060	0.055	658.8	8.6
Lungs	0.060	0.056	671.6	8.8

Table 2. Dose equivalent in rat tissues protected by spherical shielding, exposed to SPE and GCR environments. The unit for GCR dose equivalent is cSv/day, and the unit for SPE dose equivalent is cSv/event.

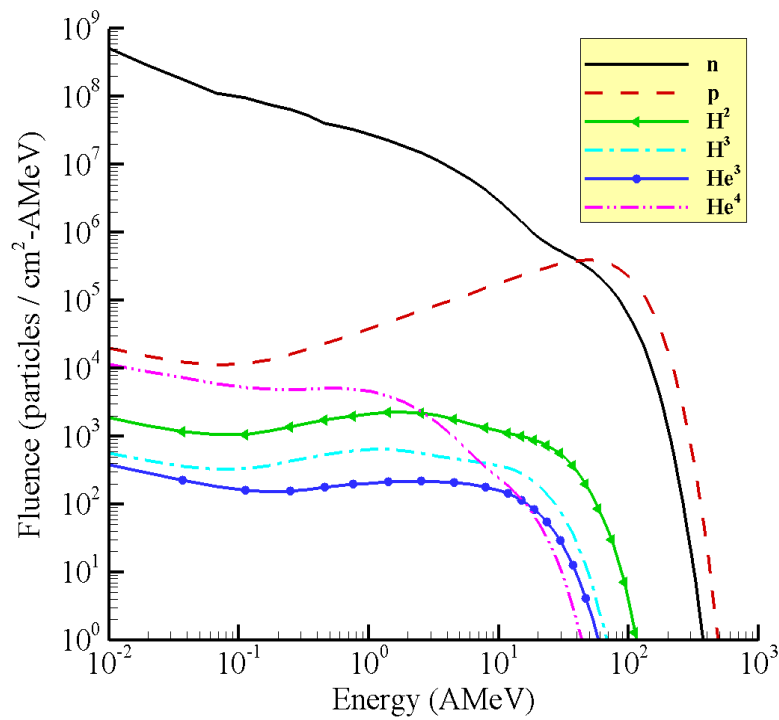|	1977 solar min GCR		August 1972 King SPE	
	0.4 g/cm^2	20 g/cm^2	0.4 g/cm^2	20 g/cm^2
BFO	0.248	0.174	1204.5	22.8
Brain	0.261	0.163	1651.7	20.7
Liver	0.244	0.158	1003.5	17.1
Lungs	0.245	0.159	1021.4	17.4

Figure 5. Neutron and light ion fluences in the rat BFO protected by 20 g/cm^2 of aluminum and exposed to the August 1972 King SPE.
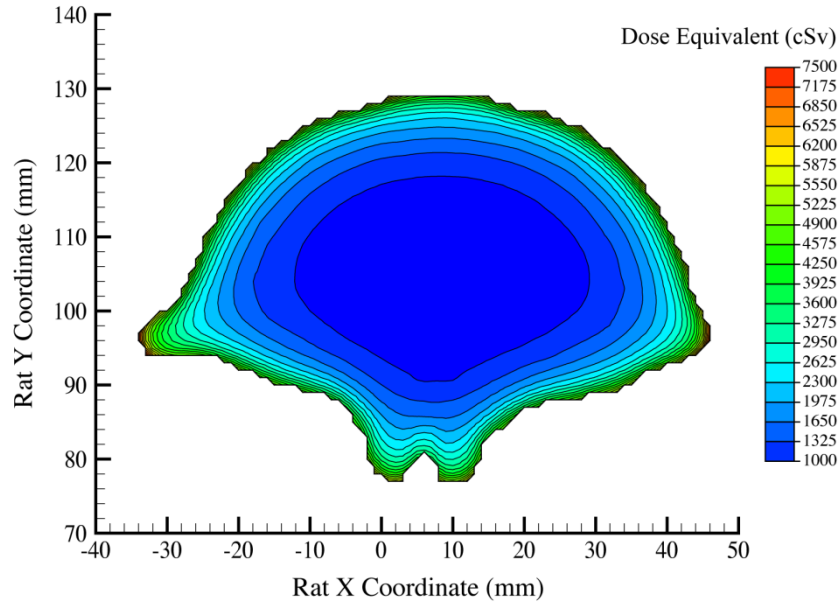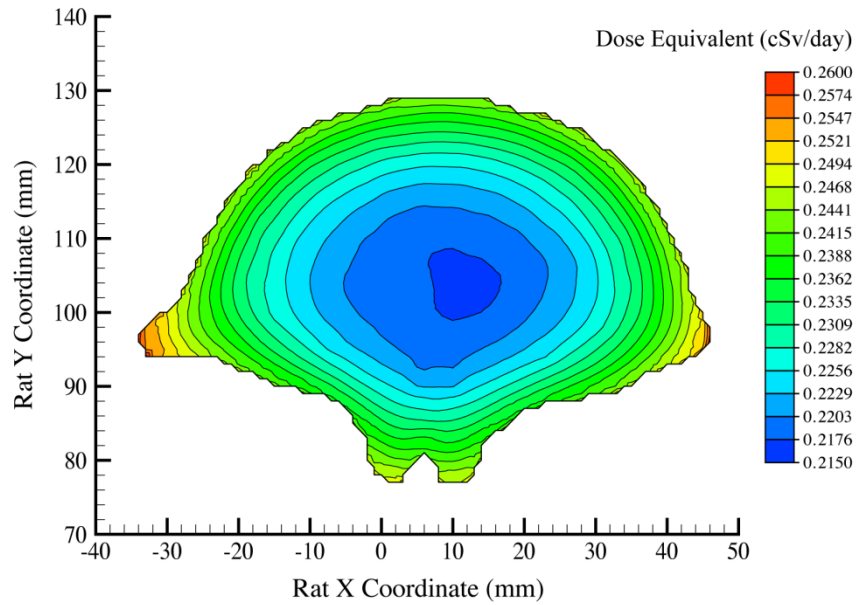
Figure 6. Contour plot of dose equivalent within a single rat cross section, calculated at points in a regularly spaced 1 mm grid. Analysis included 0.4 g/cm^2 of aluminum shielding and the August 1972 King SPE.

Figure 7. Contour plot of dose equivalent within a single rat cross section, calculated at points in a regularly spaced 1 mm grid. Analysis included 0.4 g/cm^2 of aluminum shielding and the 1977 solar minimum GCR spectrum of O'Neill and Badhwar.

6. References

Cucinotta, F.A., Kim, M.Y., Ren, L., Evaluating Shielding Effectiveness for Reducing Space
Radiation Cancer Risks. Radiation Measurements, Volume 41, pp. 1173-1185 (2006).

King, J.H., Solar Proton Fluences for 1977-1983 Space Missions. Journal of Spacecraft and Rockets,
Volume 11, pp. 401-408 (1974).

Kramer, R., Vieira, J.W., Khoury, H.J., Lima, F.R.A., Fuelle, D., All about MAX: A Male Adult Voxel
Phantom for Monte Carlo Calculations in Radiation Protection Dosimetry. Physics in Medicine
and Biology, Volume 48, pp. 1239-1262 (2003).

Kramer, R., Vieira, J.W., Khoury, H.J., Lima, F.R.A., Loureiro, E.C.M., Lima, V.J.M., Hoff, G., All about
FAX: A Female Adult Voxel Phantom for Monte Carlo Calculations in Radiation Protection
Dosimetry. Physics in Medicine and Biology, Volume 49, pp. 5203-5216 (2004).

O'Neill, P.M., Badhwar-O'Neill, Galactic Cosmic Ray Model Update Based on Advanced Composition
Explorer (ACE) Energy Spectra from 1997 to Present. Advances in Space Research, Volume 37,
pp. 1727-1733 (2006).

Persson, P.O., Strang, G., A Simple Mesh Generator in MATLAB. Society for Industrial and Applied
Mathematics Review, Volume 46, pp. 329-345 (2004).

Poole, Trevor B, editor, The UFAW Handbook on the Care & Management of Laboratory Animals.
6th ed, Longman Scientific & Technical, England (1986).

Slaba, T.C., Blattnig, S.R., Clowdsley, M.S., Walker, S.A., Badavi, F.F., An Improved Neutron Transport
Algorithm for HZETRN. Submitted to Advances in Space Research (2008).

Slaba, T.C., Qualls, G.D., Clowdsley, M.S., Blattnig, S.R., Simonsen, L.C., Walker, S.A., Singleterry, R.C.,
Analysis of Mass Averaged Tissue Doses in CAM, CAF, MAX, and FAX. NASA TP 2009-
215562 (2009).

Wilson, J.W., Townsend, L.W., Schimmerling, W., Khandelwal, G.S., Khan, F., Nealy, J.E., Cucinotta,
F.A., Simonsen, L.C., Shinn, J.L., Norbury, J.W., Transport Methods and Interactions for Space
Radiations. NASA Reference Publication 1257 (1991).

Yucker, W.R., Huston, S.L., The Computerized Anatomical Female. Final Report, MDC-6107, McDonnell
Douglas Company, Huntington Beach, CA (1990).

Yucker, W.R., Reck, R.J., Computerized Anatomical Female Body Self-Shielding Distributions. Report,
MDC 92H0749, McDonnell Douglas Company, Huntington Beach, CA (1992).

Zaidi, H., Xu, X.G., Computational Anthropomorphic Models of the Human Anatomy: The Path to
Realistic Monte Carlo Modeling in Radiological Sciences. Annual Review of Biomedical
Engineering, Volume 9, pp. 471-500 (2007).

1. REPORT DATE *(DD-MM-YYYY)*	2. REPORT TYPE	3. DATES COVERED *(From - To)*
01-03-2010	Technical Publication	

4. TITLE AND SUBTITLE

A Rat Body Phantom for Radiation Analysis

5a. CONTRACT NUMBER

5b. GRANT NUMBER

5c. PROGRAM ELEMENT NUMBER

6. AUTHOR(S)

Qualls, Garry D.; Clowdsley, Martha S.; Slaba, Tony C.; Walker, Steven A.

5d. PROJECT NUMBER

5e. TASK NUMBER

5f. WORK UNIT NUMBER

651549.02.07.01

7. PERFORMING ORGANIZATION NAME(S) AND ADDRESS(ES)

NASA Langley Research Center
Hampton, VA 23681-2199

8. PERFORMING ORGANIZATION REPORT NUMBER

L-19845

9. SPONSORING/MONITORING AGENCY NAME(S) AND ADDRESS(ES)

National Aeronautics and Space Administration
Washington, DC 20546-0001

10. SPONSOR/MONITOR'S ACRONYM(S)

NASA

11. SPONSOR/MONITOR'S REPORT NUMBER(S)

NASA/TP-2010-216212

12. DISTRIBUTION/AVAILABILITY STATEMENT

Unclassified - Unlimited
Subject Category 93
Availability: NASA CASI (443) 757-5802

13. SUPPLEMENTARY NOTES

14. ABSTRACT

To reduce the uncertainties associated with estimating the biological effects of ionizing radiation in tissue, researchers rely on laboratory experiments in which mono-energetic, single specie beams are applied to cell cultures, insects, and small animals. To estimate the radiation effects on astronauts in deep space or low Earth orbit, who are exposed to mixed field broad spectrum radiation, these experimental results are extrapolated and combined with other data to produce radiation quality factors, radiation weighting factors, and other risk related quantities for humans. One way to reduce the uncertainty associated with such extrapolations is to utilize analysis tools that are applicable to both laboratory and space environments. The use of physical and computational body phantoms to predict radiation exposure and its effects is well established and a wide range of human and non-human phantoms are in use today. In this paper, a computational rat phantom is presented, as well as a description of the process through which that phantom has been coupled to existing radiation analysis tools. Sample results are presented for two space radiation environments.

15. SUBJECT TERMS

Space Radiation; Body phantom; CT scan; Radiation effects; Radiation transport; Rats; Ray tracing

16. SECURITY CLASSIFICATION OF:			17. LIMITATION OF ABSTRACT	18. NUMBER OF PAGES	19a. NAME OF RESPONSIBLE PERSON
a. REPORT	b. ABSTRACT	c. THIS PAGE			STI Help Desk (email: help@sti.nasa.gov)
U	U	U	UU	18	19b. TELEPHONE NUMBER *(Include area code)* (443) 757-5802